JOURNAL OF MAGNETIC RESONANCE IMAGING 13:534–546 (2001)

Original Research

Diffusion Tensor Imaging: Concepts and Applications

Denis Le Bihan, MD, PhD,[1]* Jean-François Mangin, PhD,[1] Cyril Poupon, PhD,[1] Chris A. Clark, PhD,[1] Sabina Pappata, MD, PhD,[1] Nicolas Molko, MD,[1,2] and Hughes Chabriat, MD[1,2]

The success of diffusion magnetic resonance imaging (MRI) is deeply rooted in the powerful concept that during their random, diffusion-driven displacements molecules probe tissue structure at a microscopic scale well beyond the usual image resolution. As diffusion is truly a three-dimensional process, molecular mobility in tissues may be anisotropic, as in brain white matter. With diffusion tensor imaging (DTI), diffusion anisotropy effects can be fully extracted, characterized, and exploited, providing even more exquisite details on tissue microstructure. The most advanced application is certainly that of fiber tracking in the brain, which, in combination with functional MRI, might open a window on the important issue of connectivity. DTI has also been used to demonstrate subtle abnormalities in a variety of diseases (including stroke, multiple sclerosis, dyslexia, and schizophrenia) and is currently becoming part of many routine clinical protocols. The aim of this article is to review the concepts behind DTI and to present potential applications. J. Magn. Reson. Imaging 2001;13: 534–546. © 2001 Wiley-Liss, Inc.

THE BASIC PRINCIPLES of diffusion MRI were introduced in the mid-1980s (1–3); they combined NMR imaging principles with those introduced earlier to encode molecular diffusion effects in the NMR signal by using bipolar magnetic field gradient pulses (4). Molecular diffusion refers to the random translational motion of molecules, also called Brownian motion, that results from the thermal energy carried by these molecules. The success of diffusion MRI is deeply rooted in the powerful concept that during their random, diffusion-driven displacements molecules probe tissue structure at a microscopic scale well beyond the usual image resolution: during typical diffusion times of about 50 msec, water molecules (water is the most convenient molecular species to study with diffusion MRI, but some metabolites may also be studied) move in the brain on average over distances around 10 μm, bouncing, crossing, or interacting with many tissue components such as cell membranes, fibers, or macromolecules.

The overall effect observed in a diffusion MRI image voxel of several mm^3 reflects, on a statistical basis, the displacement distribution of the water molecules present within this voxel. The observation of this displacement distribution may thus provide unique clues to the structure and geometric organization of tissues. MRI is the only means we have to observe diffusion in vivo noninvasively. Furthermore, MRI provides access to both superficial and deep organs with high resolution and does not interfere with the diffusion process itself: diffusion is an intrinsic physical process that is totally independent of the MR effect or the magnetic field. This is not the case for most MRI-accessible parameters, such as T1 or T2.

Potential clinical applications of water diffusion MRI were suggested very early (5). The most successful application of diffusion MRI since the early 1990s has been brain ischemia (6), following the discovery in cat brain by Moseley et al. that water diffusion drops at a very early stage of the ischemic event (7). Diffusion MRI provides some patients with the opportunity to receive suitable treatment at a stage when brain tissue might still be salvageable.

Furthermore, diffusion is truly a three-dimensional process. Hence, molecular mobility in tissues may not be the same in all directions. This anisotropy may result from a peculiar physical arrangement of the medium (such as in liquid crystals) or the presence of obstacles that limit molecular movement in some directions. As diffusion is encoded in the MRI signal by using magnetic field gradient pulses (8), only molecular displacements that occur along the direction of the gradient are visible. The effect of diffusion anisotropy can then easily be detected by observing variations in the diffusion measurements when the direction of the gradient pulses is changed. This is a unique, powerful feature not found with usual MRI parameters, such as T1 or T2.

Diffusion anisotropy had been observed long ago in muscle (9). With the advent of diffusion MRI, anisotropy was also detected in vivo at the end of the 1980s in spinal cord (10) and brain white matter (11,12). More recently, diffusion anisotropy has also been seen in rat brain gray matter (13,14) and in human brain of neo-

[1]Service Hospitalier Frédéric Joliot, CEA, 91406 Orsay, France.
[2]Department of Neurology, Lariboisière Hospital, 75010 Paris, France.
*Address reprint requests to: D.L.B., Service Hospitalier Frédéric Joliot, CEA, 4, place du Général Leclerc, 91406 Orsay Cedex France. E-mail: lebihan@shfj.cea.fr
Received July 24, 2000; Accepted August 14, 2000.

nates. Diffusion anisotropy in white matter originates from its specific organization in bundles of more or less myelinated axonal fibers running in parallel, although the exact mechanism is still not completely understood (see below): diffusion in the direction of the fibers is faster than in the perpendicular direction. It quickly appeared that this feature could be exploited to map out the orientation in space of the white matter tracks in the brain using a color scale, assuming that the direction of the fastest diffusion would indicate the overall orientation of the fibers (15).

This pioneering work on diffusion anisotropy really took off with the introduction of the more rigorous formalism of the *diffusion tensor* by Basser et al. (16–18). With diffusion tensor imaging (DTI), diffusion anisotropy effects in diffusion MRI data could be fully extracted, characterized, and exploited, providing even more exquisite details of tissue microstructure. Many studies have been published dealing with the optimization of the MRI sequences necessary to gain access to the diffusion tensor, the processing and display of DTI data, and, of course, potential applications. The most advanced application is certainly that of fiber tracking in the brain, which, in combination with functional MRI, might open a window onto the important issue of connectivity.

The aim of this article is to review the concepts behind DTI and to present potential applications.

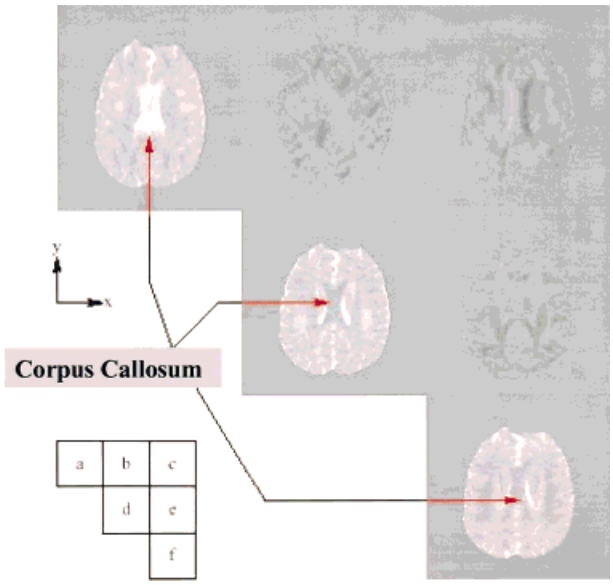

Figure 1. The diffusion tensor, axial slices. Diffusivity along x, y, and z axes, shown in D_{xx} (**a**), D_{yy} (**d**), and D_{zz} (**f**) images, respectively, is clearly different in white matter, especially in the corpus callosum. Nondiagonal images [D_{xy} (**b**), D_{xz} (**c**), and D_{yz} (**e**)] are not noise images because the x, y, z reference frame of the MRI scanner does not coincide with the diffusion reference frame of tissues in most voxels.

DIFFUSION TENSOR MRI: DATA ACQUISITION AND PROCESSING

The Diffusion Tensor

With plain diffusion MRI, diffusion is fully described using a single (scalar) parameter, the diffusion coefficient, D. The effect of diffusion on the MRI signal (most often a spin-echo signal) is an attenuation, A, which depends on D and on the "b factor," which characterizes the the gradient pulses (timing, amplitude, shape) used in the MRI sequence (8):

$$A = \exp(-bD). \qquad (1)$$

However, in the presence of anisotropy, diffusion can no longer be characterized by a single scalar coefficient, but requires a tensor, $\underline{\mathbf{D}}$, which fully describes molecular mobility along each direction and correlation between these directions (4) (Fig. 1):

$$\underline{\mathbf{D}} = \begin{matrix} D_{xx} & D_{xy} & D_{xz} \\ D_{yx} & D_{yy} & D_{yz} \\ D_{zx} & D_{zy} & D_{zz} \end{matrix}. \qquad (2)$$

This tensor is symmetric ($D_{ij} = D_{ji}$, with $i, j = x, y, z$).

In a reference frame [x', y', z'] that coincides with the principal or self directions of diffusivity, the off-diagonal terms do not exist, and the tensor is reduced only to its diagonal terms, $D_{x'x'}$, $D_{y'y'}$, $D_{z'z'}$, which represent molecular mobility along axes x', y', and z', respectively. The echo attenuation then becomes:

$$A = \exp(-b_{x'x'}D_{x'x'} - b_{y'y'}D_{y'y'} - b_{z'z'}D_{z'z'}) \qquad (3)$$

where b_{ii} are the elements of the $\underline{\mathbf{b}}$ matrix (which now replaces the b factor) expressed in the coordinates of this reference frame.

In practice, unfortunately, measurements are made in the reference frame [x, y, z] of the MRI scanner gradients, which usually does not coincide with the diffusion frame of the tissue. Therefore, one must also consider the coupling of the nondiagonal elements, b_{ij}, of the $\underline{\mathbf{b}}$ matrix with the nondiagonal terms, D_{ij}, ($i \neq j$), of the diffusion tensor (now expressed in the scanner frame), which reflect correlation between molecular displacements in perpendicular directions (17):

$$A = \exp\left(-\sum_{i=x,y,z}\sum_{j=x,y,z} \underline{\mathbf{b}}_{ij}\underline{\mathbf{D}}_{ij}\right) \qquad (4)$$

or

$$A = \exp(-b_{xx}D_{xx} - b_{yy}D_{yy} - b_{zz}D_{zz} - 2b_{xy}D_{xy} - 2b_{xz}D_{xz} - 2b_{yz}D_{yz}). \qquad (5)$$

Hence, it is important to note that by using diffusion-encoding gradient pulses along one direction only, say x, signal attenuation not only depends on the diffusion effects along this direction but may also include contribution from other directions, say y and z.

Calculation of $\underline{\mathbf{b}}$ may quickly become complicated when many gradient pulses are used (20,21), but the full determination of the diffusion tensor is necessary if one wants to assess properly and fully all anisotropic diffusion effects.

DTI Data Acquisition

To determine the diffusion tensor fully, one must first collect diffusion-weighted images along several gradient directions, using diffusion-sensitized MRI pulse sequences (22) such as echoplanar imaging (EPI). As the diffusion tensor is symmetric, measurements along only six directions are mandatory (instead of nine), along with an image acquired without diffusion weighting ($b = 0$). A typical set of gradient combinations that preserves uniform space sampling and similar b values along each direction is as follows (coefficients for gradient pulses along the (x, y, z) axes, normalized to a given amplitude, G):

$$[(1/\sqrt{2},\ 0,\ 1/\sqrt{2});\ (-1/\sqrt{2},\ 0,\ 1/\sqrt{2});$$
$$(0,\ 1/\sqrt{2},\ 1/\sqrt{2});\ (0,\ 1/\sqrt{2},\ -1/\sqrt{2});$$
$$(1/\sqrt{2},\ 1/\sqrt{2},\ 0);\ (-1/\sqrt{2},\ 1/\sqrt{2},\ 0)].$$

This minimal set of images may be repeated for averaging, as the signal-to-noise ratio (SNR) may be low (17,18). Note that it is not necessary (and not efficient in terms of SNR) to obtain data with different b values for each direction. A simple calculation (22) shows that, in the case of scalar diffusion, one gets the best accuracy on the diffusion coefficient, D, from two acquisitions when using 2 b factors, b_1 and b_2, differing by about $1/D$ (23). In the brain, this translates to $(b_2 - b_1) \approx$ 1000–1500 s/mm^2. If more than two acquisitions are to be used (for averaging purposes), error propagation theory (24) shows that it is better to accumulate n_1 and n_2 measurements at each of the low and high b factors, b_1 and b_2, than to use a range of b factors. The accuracy dD/D is then obtained from the raw image SNR:

$$dD/D = [1/n_1 + \exp[2D(b_1 - b_2)]/n_2]^{1/2} \times [\mathrm{SNR} \cdot D(b_1 - b_2)]. \quad (6)$$

In the anisotropic case, this paradigm would be still useful, but one should bear in mind that D will change for each voxel according to the measurement direction (25).

Acquisition performed with linear sets of b value ranges remains, however, extremely useful to assess the sequence/hardware performance (stability, eddy currents, . . .) (22) or to characterize the diffusion process better, in particular in the presence of multiple diffusion compartments (see below).

In the case of axial symmetry, only four directions are necessary (tetrahedral encoding) (26), as suggested in the spinal cord (27,28). The acquisition time and the number of images to process are then reduced. In contrast, efforts are now being made to collect data along as many directions in space as possible to avoid sampling direction biases. This uniform space sampling paradigm is particularly interesting for fiber tracking applications and provides a gain in SNR (25,29) (Fig. 2 and see below).

DTI Data Processing

A second step is to estimate the D_{ij} values from the set of diffusion/orientation-weighted images, generally by multiple linear regression, using Eq. [5]. From the diffusion tensor components, one may calculate indices that reflect either the average diffusion or the degree of anisotropy in each voxel (see below). Another step is to determine the main direction of diffusivities in each voxel and the diffusion values associated with these directions. This is equivalent to determining the reference frame [x', y', z'] where the off-diagonal terms of **D** are null. This "diagonalization" of the diffusion tensor provides eigen-vectors and eigen-values, λ, which correspond respectively to the main diffusion directions and associated diffusivities (17,18). (The eigen-diffusivities, λ, are not to be confused with the tortuosity factors.)

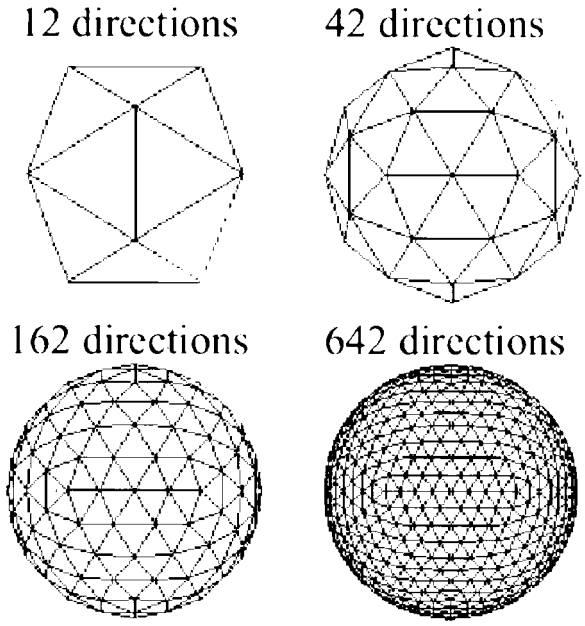

Figure 2. Schemes for directional sampling. Although initial sampling schemes consisted of six (or even four) directions of measurements, progress is made in scanning space more uniformly along many directions, especially for fiber orientation mapping.

As it is difficult to display tensor data with images (multiple images would be necessary), the concept of *diffusion ellipsoids* has been proposed (17,18). An ellipsoid is a three-dimensional representation of the diffusion distance covered in space by molecules in a given diffusion time, T_d. These ellipsoids, which can be displayed for each voxel of the image, are easily calculated from the eigen diffusivities, λ_1, λ_2, and λ_3 (corresponding to $D_{x'x'}$, $D_{y'y'}$, and $D_{z'z'}$):

$$x'^2/(2\lambda_1 T_d) + y'^2/(2\lambda_2 T_d) + z'^2/(2\lambda_3 T_d) = 1 \quad (7)$$

where x', y', and z' refer to the frame of the main diffusion direction of the tensor. These eigen diffusivities represent the unidimensional diffusion coefficients in the main directions of diffusivities of the medium. Therefore, the main axis of the ellipsoid gives the main diffusion direction in the voxel (coinciding with the direction of the fibers), while the eccentricity of the ellipsoid provides information about the degree of anisot-

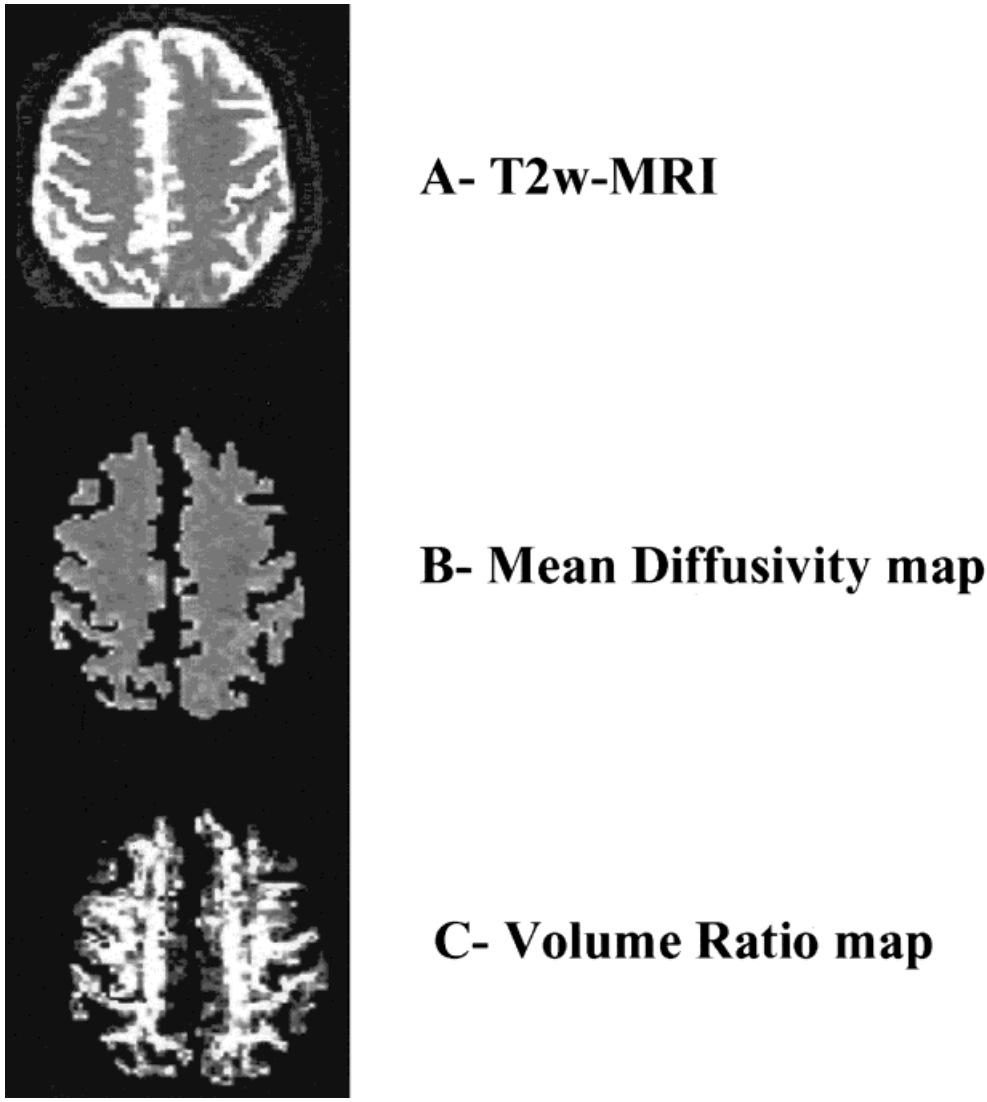

Figure 3. DTI in normal brain. The mean diffusivity (obtained from the trace of the diffusion tensor) corresponds to the overall water molecular displacements, which are very similar in gray and white matter. On the other hand, the volume ratio index, which reflects anisotropy, varies greatly in gray and white matter. Anisotropy is mainly seen in highly oriented white matter tracks.

ropy and its symmetry. (Isotropic diffusion would be seen as a sphere.) The length of the ellipsoids in any direction in space is given by the diffusion distance covered in this direction. In other words, the ellipsoid can also be seen as the three-dimensional surface of constant mean squared displacement of the diffusing molecules.

Recent work has demonstrated the feasibility of DTI in animal models, as well as in the human brain (16,26,30,31).

EXTRACTING INFORMATION FROM DTI DATA

Using DTI, it appears that diffusion data can be analyzed in three ways to provide information on tissue microstructure and architecture for each voxel (32,33): The mean diffusivity, which characterizes the overall mean-squared displacement of molecules (average ellipsoid size) and the overall presence of obstacles to diffusion; the degree of anisotropy, which describes how much molecular displacements vary in space (ellipsoid eccentricity) and is related to the presence of oriented structures; and the main direction of diffusivities (main ellipsoid axes), which is linked to the orientation in space of the structures. These three DTI meta-parameters can all be derived from the whole knowledge of the diffusion tensor. However, due to the complexity of data acquisition and processing for full DTI, and the sensitivity to noise of the determination of the diffusion tensor eigen-values, simplified approaches have been proposed.

Mean Diffusivity

To obtain an overall evaluation of the diffusion in a voxel or region, one must avoid anisotropic diffusion effects and limit the result to an *invariant,* ie, a quantity that is independent of the orientation of the reference frame (18). Among several combinations of the tensor elements, the trace of the diffusion tensor,

$$\mathrm{Tr}(\underline{\mathbf{D}}) = D_{xx} + D_{yy} + D_{zz} \qquad (8)$$

is such an invariant. The mean diffusivity is then given by $\mathrm{Tr}(\underline{\mathbf{D}})/3$. A slightly different definition of the trace has

proved useful in assessing the diffusion drop in brain ischemia (34) (Fig. 3 and see below).

Unfortunately, the correct estimation of Tr(**D**) still requires the complete determination of the diffusion tensor. Generally, one cannot simply add diffusion coefficients obtained by separately acquiring data with gradient pulses added along *x*, *y*, and *z* axes, as these measured coefficients usually do not coincide with D_{xx}, D_{yy}, and D_{zz}, respectively (see above). The reason is that the diffusion attenuation that results, for instance, from inserting gradients on the *x* axis (see above) is not simply $A = \exp[-b_{xx}D_{xx}]$, unless diffusion is isotropic (no nondiagonal terms) or the contribution of the gradient pulses on *y* and *z* axes is negligible. (Sequences can be written that way.)

To avoid this problem and to simplify the approach, several groups have designed sequences based on multiple echoes or acquisitions with tetrahedral gradient configurations, so as to cancel nondiagonal term contributions to the MRI signal directly (26,35–37).

Diffusion Anisotropy Indices

Several scalar indices have been proposed to characterize diffusion anisotropy. Initially, simple indices calculated from diffusion-weighted images (10) or ADCs obtained in perpendicular directions were used, such as ADC*x*/ADC*y* (15) and displayed using a color scale. Other groups have devised indices mixing measurements along *x*, *y*, and *z* directions, such as max[ADC*x*, ADC*y*, ADC*z*]/min[ADC*x*, ADC*y*, ADC*z*] or the standard deviation of ADC*x*, ADC*y*, and ADC*z* divided by their mean value (34). Unfortunately, none of these indices are really quantitative, as they do not correspond to a single meaningful physical parameter and, more importantly, are clearly dependent on the choice of directions made for the measurements. The degree of anisotropy would then vary according to the respective orientation of the gradient hardware and the tissue frames of reference and would generally be underestimated. Here again, invariant indices must be found to avoid such biases and provide an objective, intrinsic structural information (38).

Invariant indices are thus made of combinations of the terms of the diagonalized diffusion tensor, ie, the eigen-values λ_1, λ_2, and λ_3. The most commonly used invariant indices are the relative anisotropy (RA), the fractional anisotropy (FA), and the volume ratio (VR) indices, defined respectively as:

$$\mathrm{RA} = \sqrt{(\lambda_1 - \langle\lambda\rangle)^2 + (\lambda_2 - \langle\lambda\rangle)^2 + (\lambda_3 - \langle\lambda\rangle)^2}/\sqrt{3\langle\lambda\rangle} \tag{9}$$

where

$$\langle\lambda\rangle = (\lambda_1 + \lambda_2 + \lambda_3)/3. \tag{10}$$

$$\mathrm{FA} = \sqrt{3[(\lambda_1 - \langle\lambda\rangle)^2 + (\lambda_2 - \langle\lambda\rangle)^2 + (\lambda_3 - \langle\lambda\rangle)^2]}/\sqrt{2(\lambda_1^2 + \lambda_2^2 + \lambda_3^2)}. \tag{11}$$

$$\mathrm{VR} = \lambda_1\lambda_2\lambda_3/\langle\lambda\rangle^3. \tag{12}$$

RA, a normalized standard deviation, also represents the ratio of the anisotropic part of **D** to its isotropic part. FA measures the fraction of the "magnitude" of **D** that can be ascribed to anisotropic diffusion. FA and RA vary between 0 (isotropic diffusion) and 1($\sqrt{2}$ for RA) (infinite anisotropy). As for VR, which represents the ratio of the ellipsoid volume to the volume of a sphere of radius $\langle\lambda\rangle$, its range is from 1 (isotropic diffusion) to 0, so that some authors prefer to use (1 − VR) (39).

Once these indices have been defined, it is possible to evaluate them directly from diffusion-weighted images, ie, without the need to calculate the diffusion tensor (40). For instance, A_σ, which is very similar to RA, has been proposed as (41):

$$A_\sigma = \sqrt{\sum_{i=x,y,z} (D_i - \langle D\rangle)^2 + (D_{xy}^2 + D_{xz}^2 + D_{yz}^2)}/\sqrt{6\langle D\rangle} \tag{13}$$

with

$$\langle D\rangle = \sum_{i=x,y,z} D_i/3 \tag{14}$$

Also, images directly sensitive to anisotropy indices, or anisotropically weighted images, can be obtained (42). Finally, the concept of these *intravoxel* anisotropy indices can be extended to a family of *intervoxel* or "lattice" measures of diffusion anisotropy, which allows neighboring voxels to be considered together, in a region of interest, without losing anisotropy effects resulting from different fiber orientations across voxels (39). Clinically relevant images of anisotropy indices have been obtained in the human brain (31,43) (Figs. 3, 4; Table 1).

Fiber Orientation Mapping

The last family of parameters that can be extracted from the DTI concept relates to the mapping of the orientation in space of tissue structure. The assumption is that the direction of the fibers is colinear with the direction of the eigen-vector associated with the largest eigen diffusivity. This approach opens a completely new way to gain direct and in vivo information on the organization in space of oriented tissues, such as muscle, myocardium, and brain or spine white matter, which is of considerable interest, clinically and functionally. Direction orientation can be derived from DTI directly from diffusion/orientation-weighted images or through the calculation of the diffusion tensor. A first issue is to display fiber orientation on a voxel-by-voxel basis. The use of color maps has first been suggested (15), followed by representation of ellipsoids (18,39), octahedra (44), or vectors pointing in the fiber direction (45,46) (Figs. 5, 6).

APPLICATIONS

It is important to notice that diffusion imaging is a truly quantitative method. The diffusion coefficient is a physical parameter that directly reflects the physical properties of the tissues, in terms of the random transla-

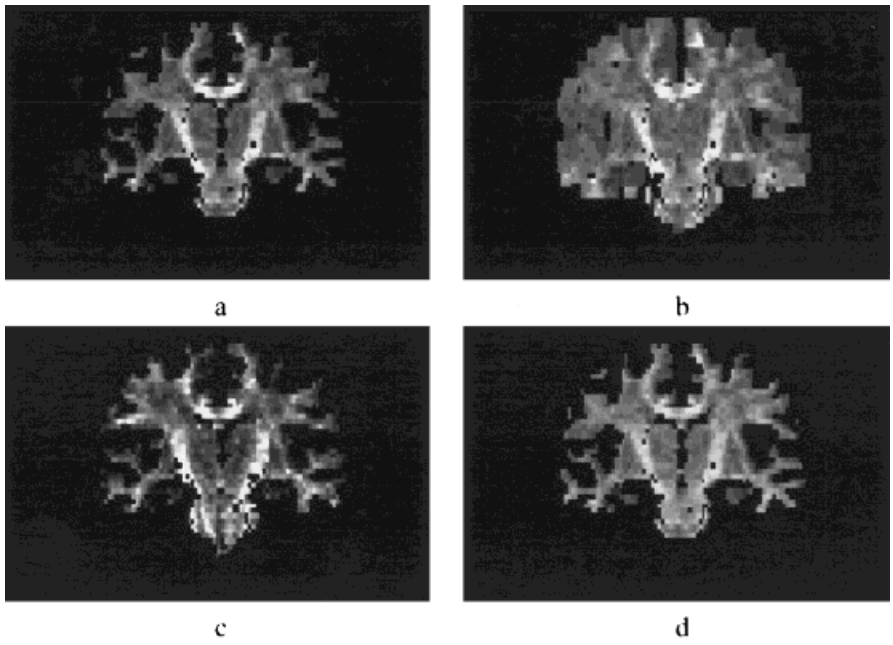

Figure 4. Comparison of various anisotropy indices. **a:** Simple anisotropy index given by: $(\lambda/\langle\lambda\rangle - 1)/2$. **b:** Relative anisotropy index (RA). **c:** Volume ratio index (VR). **d:** Fractional anisotropy index (FA).

tional movement of the molecules under study (most often water molecules, but some metabolites have been studied as well; see below). Diffusion coefficients obtained at different times in a given patient or in different patients or in different hospitals can be compared, in principle, without any need for normalization.

However, most diffusion measurements in biologic tissues refer to an apparent diffusion coefficient, and it is generally considered that diffusion in the measurement volume (voxel) has a unique diffusion coefficient. In reality, most tissues are made of multiple subcompartments, at least the intra- and the extracellular compartments, and the ADC that is measured could depend on the range used for the *b* values, as measurements with low *b* values would be more sensitive to fast diffusion components. The ideal approach would be to separate all subcompartments by fitting the data with a multiexponential decay. Unfortunately, the values for D_i are often low and not very different from each other, so that very large *b* values and very high SNRs would be required.

Table 1
Diffusion Coefficients of Water in Human Brain ($\times 10^{-3}$ mm^2/s)*

	Mean diffusivity	Anisotropy (1-volume ratio)
Cerebrospinal fluid (CSF)	3.19 ± 0.10	0.02 ± 0.01
Gray matter (frontal cortex)	0.83 ± 0.05	0.08 ± 0.05
Caudate nucleus	0.67 ± 0.02	0.08 ± 0.03
White matter		
Pyramidal tract	0.71 ± 0.04	0.93 ± 0.04
Corpus callosum (splenium)	0.69 ± 0.05	0.86 ± 0.05
Internal capsule	0.64 ± 0.03	0.70 ± 0.08
Centrum semiovale	0.65 ± 0.02	0.27 ± 0.03

*Measurements were obtained in normal volunteers using diffusion tensor MRI (from ref. 31).

Two diffusion compartments have been found in the rat brain (47). Assignment of these compartments to extra- and intracellular water is not, however, straightforward, as the values found for the two compartments are apparently opposite to the known volume fractions for the intra- and extracellular spaces (82.5% and 17.5%, respectively). This discrepancy may partially result from the exchange that occurs between compartments. It has been shown that in this case, if the residence rate in each compartment is considered, the contribution of the fast diffusing component is overestimated (48). It is thus not certain whether the two compartments that have been observed correspond to the intra- and extracellular compartments.

In any case, it is clear that the "apparent" diffusion coefficient depends on the range used for the *b* values and would not reflect univocally diffusion in the tissue. Measurements with low *b* values (less than 1000 s/mm^2) would then be more sensitive to fast diffusion components (possibly as the extracellular compartment). In clinical studies and most animal experiments, especially when data are fitted to a single exponential, diffusion patterns observed in tissues have thus to be explained by features of the extracellular space, although this compartment is physically small. Changes in the ADC calculated in these conditions should thus be interpreted in terms of changes in the diffusion coefficient of the extracellular space (tortuosity) and in its fractional volume relative to the intracellular volume. This explains why diffusion has appeared as a sensitive marker of the changes in the extracellular/intracellular volume ratio, as observed in brain ischemia, spreading depression (49–51), status epilepticus (52), and extra-physiologic manipulations of the cell size through osmotic agents (53). Using large *b* values, it could become possible to assess separately the intra- and extracellular compartments and their relative volumes, as has

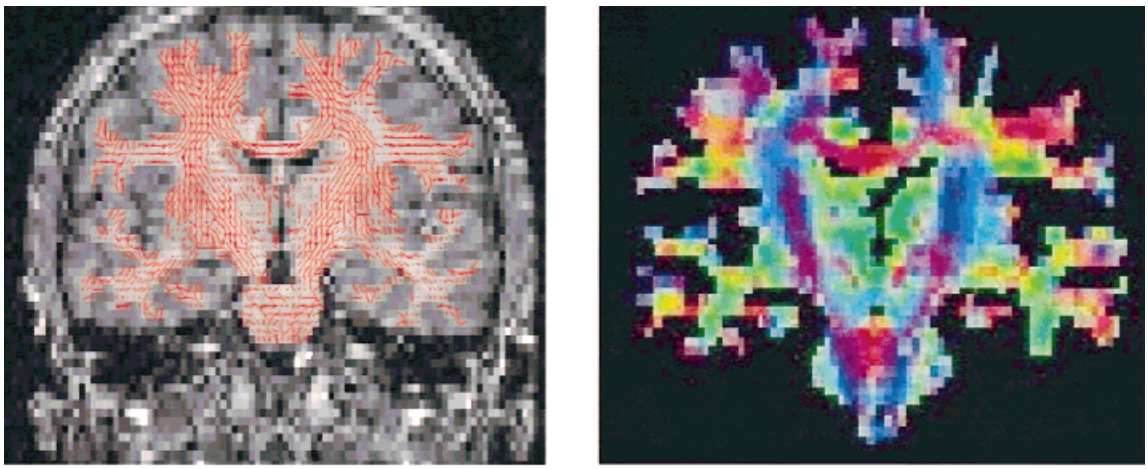

A B

Figure 5. Two-dimensional display of the diffusion tensor. **A:** Projection of the main eigen-vector on a high-resolution T2-weighted image. **B:** Representation of the main eigen-vector direction using a color scale (red = x axis, green = y axis, blue = z axis).

been suggested in vitro (54), but also in vivo in the rat (47) and human brain (55,56).

Brain Ischemia

During the acute stage of brain ischemia, water diffusion is decreased in the ischemic territory by as much as 50%, as shown in cat brain models (57). This diffusion slowdown is linked to cytotoxic edema, which results from the energetic failure of the cellular membrane Na/K pumping system. The exact mechanism of the diffusion decrease is still unclear. Increase of the slow diffusion intracellular volume fraction, changes in membrane permeability (58), and shrinkage of the extracellular space resulting in increased tortuosity for water molecules (59,60) have been suggested. Diffusion MRI has been extensively used in animal models to establish and test new therapeutic approaches. These results have been confirmed in human stroke cases, offering the potential to highlight ischemic regions within the first hours of the ischemic event, when brain tissue might still be salvageable (6,61), and well before conventional MRI becomes abnormal (vasogenic edema). Combined with perfusion MRI, diffusion MRI is under clinical evaluation as a tool to help clinicians optimize their therapeutic approach to individual patients (62), to monitor patient progress on an objective basis, and to predict clinical outcome (63–66). Anisotropic diffusion effects in diffusion-weighted images may sometimes mimic ischemic regions, especially near ventricular cavities: if diffusion sensitization is made in only one direction, which is perpendicular to the white matter fibers, bright (low diffusion) spots will be visible on the images. It is, therefore, a good practice to use images of the mean diffusivity (or the trace of the diffusion tensor) to remove these artifacts (34) (Fig. 7).

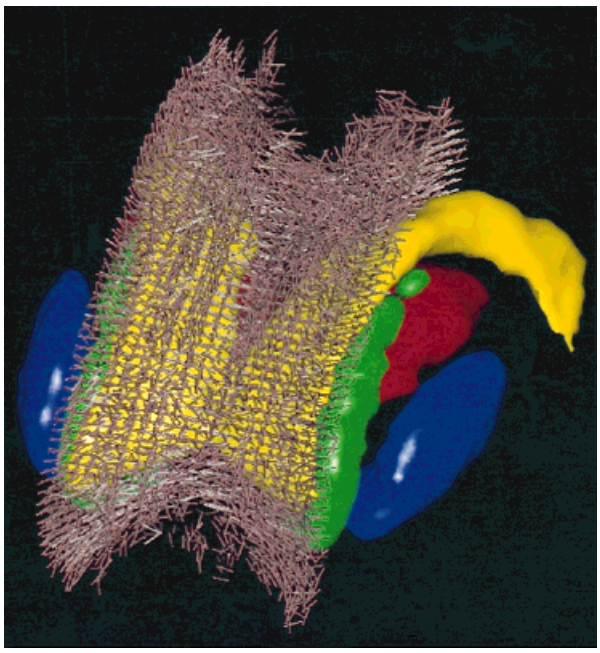

Figure 6. Three-dimensional display of the diffusion tensor. Main eigen-vectors are shown as cylinders, the length of which is scaled with the degree of anisotropy. Corpus callosum fibers are displayed around ventricles, thalami, putamen, and caudate nuclei.

Brain White Matter

In the white matter, diffusion MRI has already shown its potential in diseases such as multiple sclerosis (67). However, DTI offers more through the separation of mean diffusivity indices, such as the trace of the diffusion tensor, which reflects overall water content, and anisotropy indices, which point toward myelin fiber integrity. Examples include multiple sclerosis (68–71), leukoencephalopathy (72), Wallerian degeneration, Alz-

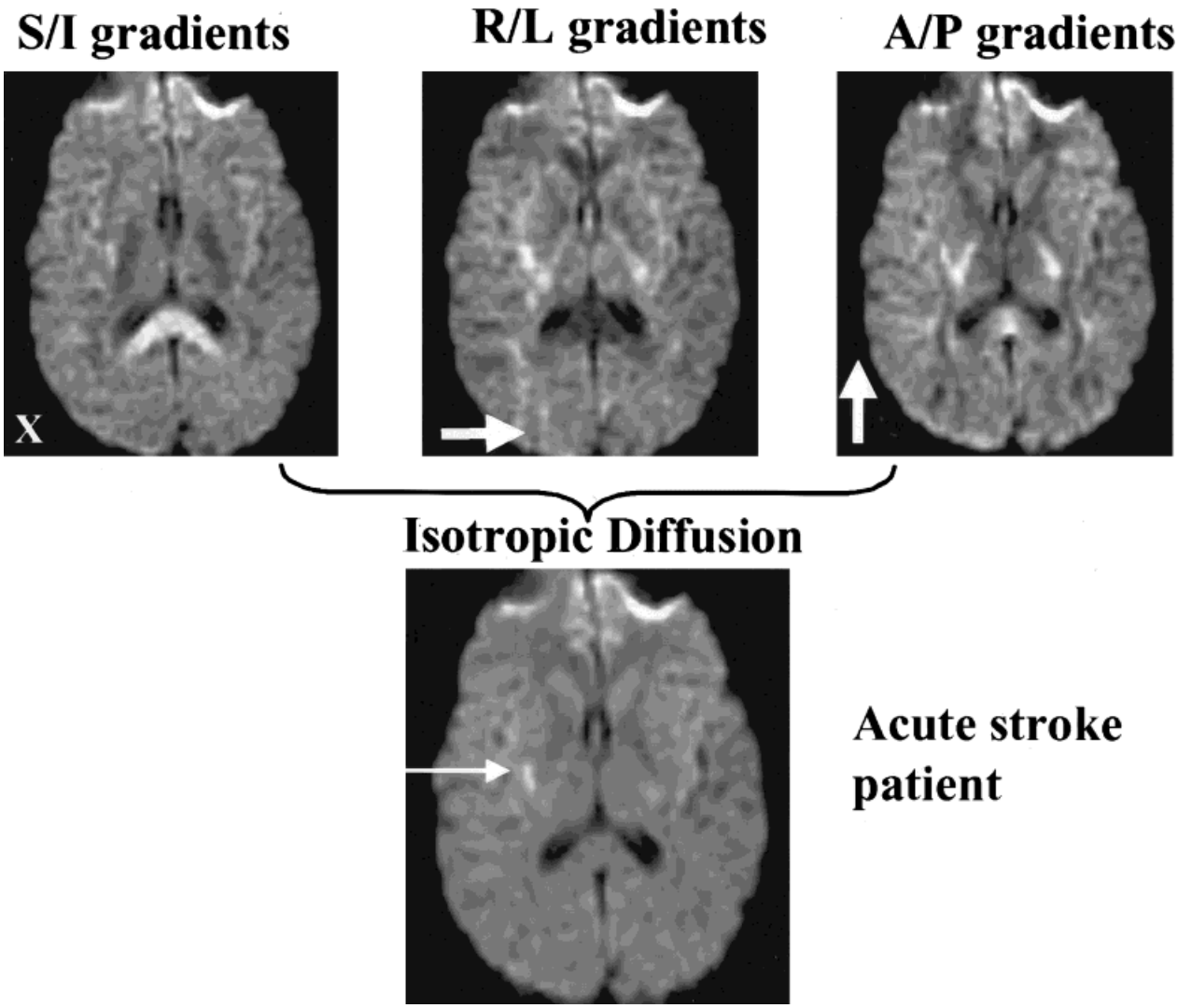

Figure 7. DTI in acute stroke (7 hours). Acute ischemic regions appear bright in diffusion-weighted images. As normal white matter regions may also appear bright in some orientations (indicated by the bold arrows) due to anisotropic diffusion effects, the use of images weighted by the trace of the diffusion tensor is more adequate (the ischemic lesion is indicated by the thin arrow). (Courtesy of C. Oppenheim, MD. Salpêtrière Hospital, Paris)

heimer's disease (73,74), and CADASIL (Cerebral Autosomal Dominant Arteriopathy with Subcortical Infarcts and Leucoenuphalopathy) (75). (Fig. 8).

It has been shown that the degree of diffusion anisotropy in white matter increases during the myelination process (43,76,77), and diffusion MRI could be used to assess brain maturation in children (78), newborns, or premature babies (43,79). Abnormal connectivity in white matter based on DTI MRI data has also been reported in frontal regions in schizophrenic patients (80,81) and in left temporo-parietal regions in dyslexic adults (82). The potential of diffusion MRI has also been studied in brain tumor grading (83–85), trauma (86), hypertensive hydrocephalus (87), AIDS (88), eclampsia (89), leukoaraiosis (90,91), migraine (92), and the spinal cord in animals (27,66,93,94) and humans (95,96).

The concepts of restriction, hindrance, tortuosity, and multiple compartments are particularly useful for understanding diffusion findings in brain white matter (33). The facts are that: a) water diffusion is highly anisotropic in white matter (10–12); b) such anisotropy has been observed even before fibers are myelinated, although to a lesser degree (43,43,77,97–102); and c) the ADCs measured in parallel and perpendicularly to the fibers do not seem to depend on the diffusion time (103,104) at least for diffusion times longer than 20 msec (Fig. 8).

Initial reports suggested that the anisotropic water diffusion could be explained on the basis that water molecules were restricted in the axons (anisotropically restricted diffusion) due to the presence of the myelin sheath (105,106). However, although restricted diffusion has been seen for intraaxonal metabolites, such as NAA (N-Acetyl-Aspartate), or for truly intraaxonal water (107), it now appears that most studies performed with relatively low *b* values are mostly sensitive to the extracellular, interaxonal space. In this condition, diffusion anisotropy in white matter should be linked to the anisotropic tortuosity of the interstitial space between fibers: diffusion is more impeded perpendicularly to the

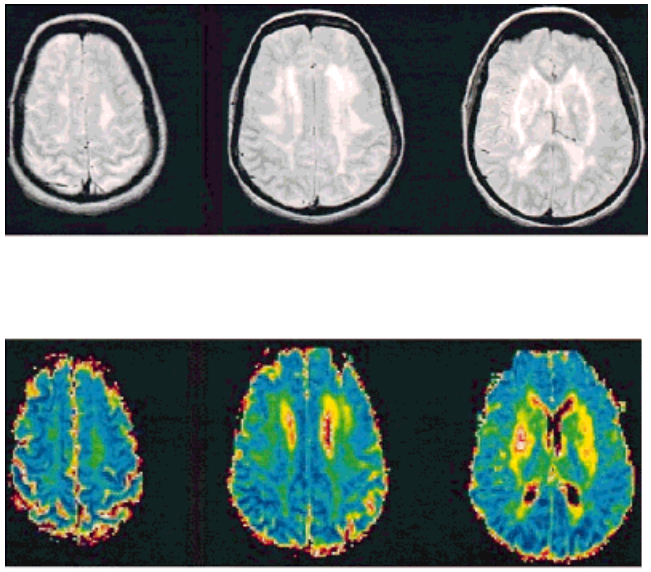

Figure 8. DTI in CADASIL, a genetic disease that results in ischemia of white matter due to abnormalities in microvasculature. White matter lesions, which appear well before clinical findings, are seen as areas with increased mean diffusivity (bottom row) in white matter regions that extend well beyond T2 abnormalities. Decreased anisotropy can also be seen on VR diffusion images (not shown). Top row, T2-weighted MRI.

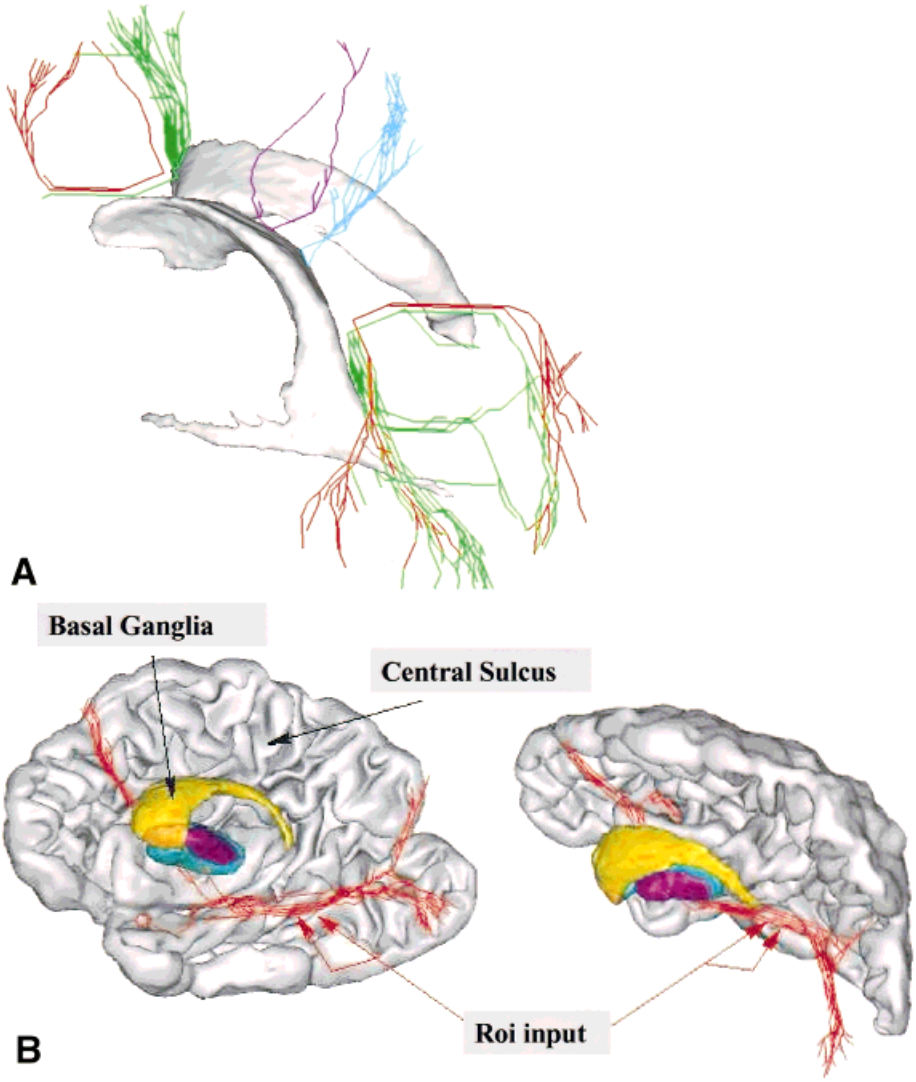

Figure 9. Brain fiber tracking. The most challenging application of DTI is brain connectivity through the visualization of white matter tracks. Using an ad hoc algorithm, it is possible to infer connectivity between neighboring principal eigen-vector voxels (as seen in Fig. 6). **A:** Callosum fibers around ventricles. **B:** Occipito-frontal tracks crossing a "seeding" region of interest (ROI input).

fibers mainly because of their geometric arrangement (103) (Fig. 7).

Considering a bundle where fibers are organized in the most compact way, molecules would have to actually travel over a distance of $\pi d/2$, where d is the fiber diameter, to apparently diffuse over a distance equal to the fiber diameter. Therefore, on average, the ADC measured perpendicularly to the fibers would then be reduced, whatever the diffusion time, to:

$$\text{ADC} = (2/\pi)^2 D_0 \approx 0.4\ D_0 \qquad (15)$$

where the reference value, D_0, is the diffusion value measured in parallel to the fibers. This ratio of about 0.4 fits reasonably well with literature data (103), although much larger ratios have been reported (39). This rough model also implies that the tortuosity factor would be anisotropic in white matter with a $\lambda_{\text{perpendicular}}/\lambda_{\text{parallel}}$ ratio of $\pi/2(\approx 1.15)$. Unfortunately, no systematic measurements of λ have been made yet in white matter using ionic extracellular tracers (108,109), although anisotropy has been seen (110). Another interesting point about this model is that it is compatible with the fact that no true restricted effects are observed when the diffusion time is increased, as there are no actual boundaries to diffusing molecules. Also, the parallel organization of the fibers may be sufficient to explain the presence of anisotropy before myelination. However, as the axonal membranes should be more permeable to water than the myelin sheaths, the degree of anisotropy should be less pronounced in the absence of myelin, as significant exchanges with the axonal spaces should occur. Oriented filaments within the axoplasm do not seem do play an important role (111).

Brain Connectivity

An important potential application of DTI is the visualization of anatomic connections between different parts of the brain on an individual basis. Studies of neuronal connectivity are tremendously important for interpreting functional MRI data and establishing how activated foci are linked together through networks (112,113). This issue is difficult, as one has to infer continuity of fiber orientation from voxel to voxel. This orientation may vary due to noisy data, and one has to deal with fiber merging, branching, dividing etc. Also, several fascicles may cross in a given voxel, which cannot be detected with the diffusion tensor approach in its present form (114). On the other hand, structures that exhibit anisotropic diffusion at the molecular level can be isotropically oriented at the microscopic level, resulting in a "powder average" effect that is difficult to resolve (115). The plot of the signal attenuation versus b may not be linear in this case (116). This deviation from linearity can be ascribed, however, to anisotropy and not to restricted diffusion, because the diffusion measurements are independent of the diffusion time. Several groups have recently approached the difficult problem of inferring connectivity from DTI data, from the dead rat brain (117) to the living human brain (118–122) (Fig. 9).

Fiber orientation mapping and connectivity studies derived from anisotropic diffusion in white matter will clearly benefit from a better understanding of the respective contributions of intraaxonal and extraaxonal compartments to anisotropy mechanisms (123).

Body

Outside the brain, diffusion has been more difficult to use successfully, because of the occurrence of strong respiratory motion artifacts in the body and the short T2 values of body tissues, which require shorter TE than in the brain and thus leave less room for the diffusion gradient pulses. These obstacles, however, can sometimes be overcome with ad hoc MR sequences and hardware. A potential for tissue characterization has been shown in the extremity muscles (124), the spine (125,126), the breast (127–129), the kidney, and the liver (130–133). As for DTI, muscle fiber orientation can be approached in organs such as the tongue (134) or the heart. Myocardium DTI (135) has the tremendous potential of providing data on heart contractility, a very important parameter, but it remains technically very challenging to perform in vivo due to heart motion.

CONCLUSIONS

Many tissue features at the microscopic level may influence NMR diffusion measurements. Many theoretical analyses on the effect of restriction, membrane permeability, hindrance, anisotropy, or tissue inhomogeneity have underlined how much care is necessary to interpret diffusion NMR data properly and infer accurate information on microstructure and microdynamics in vivo in biologic systems. Even at its current stage, DTI is the only approach available to track brain white matter fibers noninvasively. DTI should thus have a tremendous impact on brain function studies. DTI has also been used to demonstrate subtle abnormalities in a variety of diseases including multiple sclerosis and schizophrenia and is currently becoming part of many routine clinical protocols. With the development of powerful improvements to DTI, such as diffusion spectroscopy of metabolites or q-space imaging, one may expect to reach new levels and break new ground in the already flourishing field of diffusion imaging.

REFERENCES

1. Le Bihan D, Breton E. Imagerie de diffusion *in vivo* par résonance magnétique nucléaire. CR Acad Sci Paris 1985;301:1109–1112.
2. Merboldt KD, Hanicke W, Frahm J. Self-diffusion NMR imaging using stimulated echoes. J Magn Reson 1985;64:479–486.
3. Taylor DG, Bushell MC. The spatial mapping of translational diffusion coefficients by the NMR imaging technique. Phys Med Biol 1985;30:345–349.
4. Stejskal EO, Tanner JE. Spin diffusion measurements: spin echoes in the presence of a time-dependent field gradient. J Chem Phys 1965;42:288–292.
5. Le Bihan D, Breton E, Lallemand D, et al. MR imaging of intravoxel incoherent motions: application to diffusion and perfusion in neurologic disorders. Radiology 1986;161:401–407.

6. Warach S, Chien D, Li W, Ronthal M, Edelman RR. Fast magnetic resonance diffusion-weighted imaging of acute human stroke. Neurology 1992;42:1717–1723.
7. Moseley ME, Cohen Y, Mintorovitch J. Early detection of regional cerebral ischemic injury in cats: evaluation of diffusion and T2-weighted MRI and spectroscopy. Magn Reson Med 1990;14:330–346.
8. Le Bihan D. Molecular diffusion nuclear magnetic resonance imaging. Magn Reson Q 1991;7:1–30.
9. Cleveland GG, Chang DC, Hazelwood CF. Nuclear magnetic resonance measurements of skeletal muscle. Anisotropy of the diffusion coefficient of the intracellular water. Biophys J 1976;16: 1043–1053.
10. Moseley ME, Cohen Y, Kucharczyk J. Diffusion-weighted MR imaging of anisotropic water diffusion in cat central nervous system. Radiology 1990;176:439–446.
11. Chenevert TL, Brunberg JA, Pipe JG. Anisotropic diffusion within human white matter: demonstration with NMR techniques in vivo. Radiology 1990;177:401–405.
12. Turner R, Le Bihan D, Maier J, et al. Echo-planar imaging of intravoxel incoherent motions. Radiology 1990;177:407–414.
13. Lythgoe MF, Busza AL, Calamante F, et al. Effects of diffusion anisotropy on lesion delineation in a rat model of cerebral ischemia. Magn Reson Med 1997;38:662–668.
14. Hoehn Berlage M, Eis M, Schmitz B. Regional and directional anisotropy of apparent diffusion coefficient in rat brain. NMR Biomed 1999;12:45–50.
15. Douek P, Turner R, Pekar J, Patronas NJ, Le Bihan D. MR color mapping of myelin fiber orientation. J Comput Assist Tomogr 1991;15:923–929.
16. Basser PJ, Mattiello J, Turner R, Le Bihan D. Diffusion tensor echo-planar imaging of human brain. In: Proceedings of the SMRM, 1993. p 584.
17. Basser PJ, Mattiello J, Le Bihan D. Estimation of the effective self-diffusion tensor from the NMR spin echo. J Magn Reson 1994; 103:247–254.
18. Basser PJ, Mattiello J, Le Bihan D. MR diffusion tensor spectroscopy and imaging. Biophys J 1994;66:259–267.
19. Jost W. Diffusion in solids, liquids, gases, 3rd ed. San Diego: Academic Press, 1960.
20. Mattiello J, Basser PJ, Le Bihan D. Analytical expressions for the *b* matrix in NMR diffusion imaging and Spectroscopy. J Magn Reson 1994;108:131–141.
21. Mattiello J, Basser PJ, Le Bihan D. The *b*-matrix in diffusion tensor echo-planar imaging. Magn Reson Med 1997;37:292–300.
22. Le Bihan D. Diffusion and perfusion magnetic resonance imaging. Applications to functional MRI. New York: Raven Press, 1995.
23. Burdette JH, Elster AD, Ricci PE. Calculation of apparent diffusion coefficients (ADCs) in brain using two-point and six-point methods. J Comput Assist Tomogr 1998;22:792–794.
24. Xing D, Papadakis NG, Huang CL, et al. Optimised diffusion-weighting for measurement of apparent diffusion coefficient (ADC) in human brain. Magn Reson Imaging 1997;15:771–784.
25. Jones DK, Horsfield MA, Simmons A. Optimal strategies for measuring diffusion in anisotropic systems by magnetic resonance imaging. Magn Reson Med 1999;42:515–525.
26. Contouro TE, McKinstry RC, Robinson BH. Encoding of anisotropic diffusion with tetrahedral gradients: a general mathematical diffusion formalism and experiments results. Magn Reson Med 1996;35:399–412.
27. Gulani V, Iwamoto GA, Jiang H, et al. A multiple echo pulse sequence for diffusion tensor imaging and its application in excised rat spinal cords. Magn Reson Med 1997;38:868–873.
28. Clark CA, Werring DJ, Miller DH. Diffusion imaging of the spinal cord in vivo: estimation of the principal diffusivities and application to multiple sclerosis. Magn Reson Med 2000;43:133–138.
29. Papadakis NG, Xing D, Huang CLH, Hall LD, Carpenter TA. A comparative study of acquisition schemes for diffusion tensor imaging using MRI. J Magn Reson 1999;137:67–82.
30. Davis TL, Wedeen VJ, Weisskoff RM, Rose BR. White matter tract visualization by echo-planar MRI. In: Proceedings of the SMRM, 1993. p 289.
31. Pierpaoli C, Jezzard P, Basser PJ, Barnett A, DiChiro G. Diffusion tensor MR imaging of the human brain. Radiology 1996;201:637–648.
32. Basser PJ. New histological and physiological stains derived from diffusion-tensor MR images. In: Anonymous imaging: brain structure and function. New York: New York Academy of Sciences, 1997. p 123–138.
33. Le Bihan D. Molecular diffusion: tissue microdynamics and microstructure. NMR Biomed 1995;8:375–386.
34. Van Gelderen P, De Vleeschouwer MHM, Des Pres D, et al. Water diffusion and acute stroke. Magn Reson Med 1994;31:154–163.
35. Mori S, Van Zijl PCM. Diffusion weighting by the trace of the diffusion tensor within a single scan. Magn Reson Med 1995;33: 41–52.
36. Chun T, Ulug AM, Van Zijl PCM. Single-shot diffusion-weighted trace imaging on a clinical scanner. Magn Reson Med 1998;40: 622–628.
37. Hsu EW, Mori S. Analytical expressions for the NMR apparent diffusion coefficients in an arisotropic system and a simplified method for determining fiber orientation. Magn Reson Med 1995; 34:194–200.
38. Basser PJ, Pierpaoli C. Microstructural and physiological features of tissues elucidated by quantitative-diffusion-tensor MRI. J Magn Reson 1996;B111:209–219.
39. Pierpaoli C, Basser PJ. Toward a quantitative assessment of diffusion anisotropy. Magn Reson Med 1996;36:893–906.
40. Basser PJ, Pierpaoli C. A simplified method to measure the diffusion tensor from seven MR images. Magn Reson Med 1998;39: 928–934.
41. Conturo TE, McKinstry RC, Akbudak E, Robinson BH. Encoding of anisotropic diffusion with tetrahedral gradients: a general mathematical diffusion formalism and experimental results. Magn Reson Med 1996;35:399–412.
42. Shrager RI, Basser PJ. Anisotropically weighted MRI. Magn Reson Med 1998;40:160–165.
43. Neil JJ, Shiran SI, McKinstry RC, et al. Normal brain in human newborns: apparent diffusion coefficient and diffusion anisotropy measured by using diffusion tensor MR imaging. Radiology 1998; 209:57–66.
44. Gilbert RJ, Reese TG, Daftary SJ, et al. Determination of lingual myoarchitecture in whole tissue by NMR imaging of anisotropic water diffusion. Am J Physiol Gastrointest L 1998;38:G363–G369.
45. Makris N, Worth AJ, Sorensen AG, et al. Morphometry of in vivo human white matter association pathways with diffusion-weighted magnetic resonance imaging. Ann Neurol 1997;42:951–962.
46. Werring DJ, Clark CA, Barker GJ, et al. The structural and functional mechanisms of motor recovery: complementary use of diffusion tensor and functional magnetic resonance imaging in a traumatic injury of the internal capsule. J Neurol Neurosurg Psychiatry 1998;65:863–869.
47. Niendorf T, Dijkhuizen RM, Norris DG, Van Lookeren Campagne M, Nicolay K. Biexponential diffusion attenuation in various states of brain tissue: implications for diffusion-weighted imaging. Magn Reson Med 1996;36:847–857.
48. Li JG, Stanisz GJ, Henkelman RM. Integrated analysis of diffusion and relaxation of water in blood. Magn Reson Med 1998;40:79–88.
49. Latour LL, Hasegawa Y, Formato JE, Fisher M, Sotak CH. Spreading waves of decreased diffusion coefficient after cortical stimulation in the rat brain. Magn Reson Med 1994;32:189–198.
50. Hasegawa Y, Latour LL, Formato JE, Sotak CH, Fisher M. Spreading waves of a reduced diffusion coefficient of water in normal and ischemic rat brain. J Cereb Blood Flow Metab 1995;15:179–187.
51. Busch E, Hoehn Berlage M, Eis M, Gyngell ML, Hossmann KA. Simultaneous recording of EEG, DC potential and diffusion-weighted NMR imaging during potassium induced spreading depression in rats. NMR Biomed 1995;8:59–64.
52. Zhong J, Petroff OAC, Prichard JW, Gore JC. Changes in water diffusion and relaxation properties of rat cerebrum during status epilepticus. Magn Reson Med 1993;30:241–246.
53. Pfeuffer J, Flogel U, Leibfritz D. Monitoring of cell volume and water exchange time in perfused cells by diffusion-weighted H-1 NMR spectroscopy. NMR Biomed 1998;11:11–18.
54. Pilatus U, Shim H, Artemov D, et al. Intracellular volume and apparent diffusion constants of perfused cancer cell cultures, as measured by NMR. Magn Reson Med 1997;37:825–832.
55. Mulkern RV, Gudbjartsson H, Westin CF, et al. Multi-component apparent diffusion coefficients in human brain. NMR Biomed 1999;12:51–62.

56. Clark CA, Le Bihan D. Water diffusion compartmentation and anisotropy at high *b* values in human brain. In: Proceedings of the SMRM, 2000. p 759.
57. Moseley ME, Kucharczyk J, Mintorovitch J, et al. Diffusion-weighted MR imaging of acute stroke: correlation with T2-weighted and magnetic susceptibility-enhanced MR imaging in cats. AJNR 1990;11:423–429.
58. Latour LL, Svoboda K, Mitra PP, Sotak CH. Time-dependent diffusion of water in a biological model system. Proc Natl Acad Sci USA 1994;91:1229–1233.
59. Norris DG, Niendorf T, Leibfritz D. Healthy and infarcted brain tissues studied at short diffusion times: the origins of apparent restriction and the reduction in apparent diffusion coefficient. NMR Biomed 1994;7:304–310.
60. Pfeuffer J, Dreher W, Sykova E, Leibfritz D. Water signal attenuation in diffusion-weighted ^{1}H NMR experiments during cerebral ischemia: influence of intracellular restrictions, extracellular tortuosity, and exchange. Magn Reson Imaging 1998;16:1023–1032.
61. Sorensen AG, Buonanno FS, Gonzalez RG, et al. Hyperacute stroke: evaluation with combined multisection diffusion-weighted and hemodynamically weighted echo-planar MR imaging. Radiology 1996;199:391–401.
62. Warach S, Boska M, Welch KMA. Pitfalls and potential of clinical diffusion-weighted MR imaging in acute stroke. Stroke 1997;28: 481–482.
63. Lövblad KO, Baird AE, Schlaug G, et al. Ischemic lesion volumes in acute stroke by diffusion-weighted magnetic resonance imaging correlate with clinical outcome. Ann Neurol 1997;42:164–170.
64. Gonzalez RG, Schaefer PW, Buonanno FS, et al. Diffusion-weighted MR imaging: diagnostic accuracy in patients imaged within 6 hours of stroke symptom onset. Radiology 1999;210: 155–162.
65. Warach S, Boska M, Welch KM. Pitfalls and potential of clinical diffusion-weighted MR imaging in acute stroke [editorial; comment]. Stroke 1997;28:481–482.
66. Dreher W, Kahn B, Gyngell ML, et al. Temporal and regional changes during focal ischemia in rat brain studied by proton spectroscopic imaging and quantitative diffusion NMR imaging. Magn Reson Med 1998;39:878–888.
67. Ono J, Harada K, Mano T, Sakurai K, Okada S. Differentiation of dys- and demyelination using diffusional anisotropy. Pediatr Neurol 1997;16:63–66.
68. Werring DJ, Clark CA, Barker GJ, Thompson AJ, Miller DH. Diffusion tensor imaging of lesions and normal-appearing white matter in multiple sclerosis. Neurology 1999;52:1626–1632.
69. Tievsky AL, Ptak T, Farkas J. Investigation of apparent diffusion coefficient and diffusion tensor anisotropy in acute and chronic multiple sclerosis lesions. AJNR 1999;20:1491–1499.
70. Iwasawa T, Matoba H, Ogi A, et al. Diffusion-weighted imaging of the human optic nerve: a new approach to evaluate optic neuritis in multiple sclerosis. Magn Reson Med 1997;38:484–491.
71. Horsfield MA, Larsson HB, Jones DK, Gass A. Diffusion magnetic resonance imaging in multiple sclerosis. J Neurol Neurosurg Psychiatry 1998;64(suppl 1):S80–84.
72. Ay H, Buonanno FS, Schaefer PW, et al. Posterior leukoencephalopathy without severe hypertension: utility of diffusion-weighted MRI. Neurology 1998;51:1369–1376.
73. Hanyu H, Shindo H, Kakizaki D, et al. Increased water diffusion in cerebral white matter in Alzheimer's disease. Gerontology 1997; 43:343–351.
74. Hanyu H, Sakurai H, Iwamoto T, et al. Diffusion-weighted MR imaging of the hippocampus and temporal white matter in Alzheimer's disease. J Neurol Sci 1998;156:195–200.
75. Chabriat H, Papatta S, Poupon C, et al. Clinical severity in CADASIL related to ultrastructural damage in white matter—in vivo study with diffusion tensor MRI. Stroke 1999;30:2637–2643.
76. Li TQ, Chen ZG, Hindmarsh T. Diffusion-weighted MR imaging of acute cerebral ischemia. Acta Radiol 1998;39:460–473.
77. Baratti C, Barnett AS, Pierpaoli C. Comparative MR imaging study of brain maturation in kittens with T1, T2, and the trace of the diffusion tensor. Radiology 1999;210:133–142.
78. Zimmerman RA, Haselgrove JC, Wang ZY, et al. Advances in pediatric neuroimaging. Brain Dev 1998;20:275–289.
79. Huppi PS, Maier SE, Peled S, et al. Microstructural development of human newborn cerebral white matter assessed in vivo by diffusion tensor magnetic resonance imaging. Pediatr Res 1998;44: 584–590.
80. Buchsbaum MS, Tang CY, Peled S, et al. MRI white matter diffusion anisotropy and PET metabolic rate in schizophrenia. Neuroreport 1998;9:425–430.
81. Foong J, Maier M, Clark CA, et al. Neuropathological abnormalities of the corpus callosum in schizophrenia. J Neurol Neurosurg Psychiatry 2000;68:242–244.
82. Klingberg T, Hedehus M, Temple E, et al. Microstructure of temporo-parietal white matter as a basis for reading ability: evidence from diffusion tensor magnetic resonance imaging. Neuron 2000; 25:493–500.
83. Le Bihan D, Douek P, Argyropoulou M, et al. Diffusion and perfusion magnetic resonance imaging in brain tumors. Top Magn Reson Imaging 1993;5:25–31.
84. Ikezaki K, Takahashi M, Koga H, et al. Apparent diffusion coefficient (ADC) and magnetization transfer contrast (MTC) mapping of experimental brain tumor. Acta Neurochir Suppl (Wien) 1997;70: 170–172.
85. Krabbe K, Gideon P, Wagn P, et al. MR diffusion imaging of human intracranial tumours. Neuroradiology 1997;39:483–489.
86. Barzo P, Marmarou A, Fatouros P, Hayasaki K, Corwin F. Contribution of vasogenic and cellular edema to traumatic brain swelling measured by diffusion-weighted imaging. J Neurosurg 1997;87: 900–907.
87. Schwartz RB, Mulkern RV, Gudbjartsson H, Jolesz F. Diffusion-weighted MR imaging in hypertensive encephalopathy: clues to pathogenesis. AJNR 1998;19:859–862.
88. Chang L, Ernst T. MR spectroscopy and diffusion-weighted MR imaging in focal brain lesions in AIDS. Neuroimaging Clin N Am 1997;7:409–426.
89. Schaefer PW, Buonanno FS, Gonzalez RG, Schwamm LH. Diffusion-weighted imaging discriminates between cytotoxic and vasogenic edema in a patient with eclampsia. Stroke 1997;28:1082–1085.
90. Okada K, Wu LH, Kobayashi S. Diffusion-weighted MRI in severe leukoaraiosis. Stroke 1999;30:478–479.
91. Jones DK, Lythgoe D, Horsfield MA, et al. Characterization of white matter damage in ischemic leukoaraiosis with diffusion tensor MRI. Stroke 1999;30:393–397.
92. Chabriat H, Vahedi K, Clark CA, et al. Decreased hemispheric water mobility in hemiplegic migraine related to mutation of CACNA1A gene. Neurology 2000;54:510–512.
93. Ford JC, Hackney DB, Lavi E, Phillips M, Patel U. Dependence of apparent diffusion coefficients on axonal spacing, membrane permeability, and diffusion time in spinal cord white matter. J Magn Reson Imaging 1998;8:775–782.
94. Inglis BA, Yang L, Wirth ED, Plant D, Mareci TH. Diffusion anisotropy in excised normal rat spinal cord measured by NMR microscopy. Magn Reson Imaging 1997;15:441–450.
95. Clark CA, Barker GJ, Tofts PS. Magnetic resonance diffusion imaging of the human cervical spinal cord in vivo. Magn Reson Med 1999;41:1269–1273.
96. Clark CA, Werring DJ, Miller DH. Diffusion imaging in the spinal cord in vivo: estimation of the principal diffusivities and application to multiple sclerosis. Magn Reson Med 2000;43:133–138.
97. Rutherford MA, Cowan FM, Manzur AY. MR imaging of anisotropically restricted diffusion in the brain neonates and infants. J Comput Assist Tomogr 1991;15:188–198.
98. Toft PB, Leth H, Peitersen B, Lou HC, Thomsen C. The apparent diffusion coefficient of water in gray and white matter of the infant brain. J Comput Assist Tomogr 1996;20:1006–1011.
99. Vorisek I, Sykova E. Evolution of anisotropic diffusion in the developing rat corpus callosum. J Neurophysiol 1997;78:912–919.
100. Prayer D, Roberts T, Barkovich AJ, et al. Diffusion-weighted MRI of myelination in the rat brain following treatment with gonadal hormones. Neuroradiology 1997;39:320–325.
101. Takeda K, Nomura Y, Sakuma H, et al. MR assessment of normal brain development in neonates and infants: comparative study of T1- and diffusion-weighted images. J Comput Assist Tomogr 1997;21:1–7.
102. Beaulieu C, Fenrich FR, Allen PS. Multicomponent water proton transverse relaxation and T2-discriminated water diffusion in myelinated and nonmyelinated nerve. Magn Reson Imaging 1998;16: 1201–1210.
103. Le Bihan D, Turner R, Douek P. Is water diffusion restricted in human brain white matter? An echo-planar NMR imaging study. Neuroreport 1993;4:887–890.

104. Moonen CTW, Pekar J, De Vleeschouwer MHM, et al. Restricted and anisotropic displacement of water in healthy cat brain and in stroke studied by NMR diffusion imaging. Magn Reson Med 1991; 19:327–332.
105. Hajnal JV, Doran M, Hall AS. MR imaging of anisotropically restricted diffusion of water in the nervous system: technical, anatomic, and pathological considerations. J Comput Assist Tomogr 1991;15:1–18.
106. Rutherford MA, Conan FM, Manzur AY. MR imaging of anisotropically restricted diffusion in the brain of neonates and infants. Radiology 1991;180:229–233.
107. Assaf Y, Cohen Y. Detection of different water populations in brain tissue using ^{2}H single- and double-quantum-filtered diffusion NMR spectroscopy. J Magn Reson 1996;B112:151–159.
108. Nicholson C, Philipps JM. Ion diffusion modified by tortuosity and volume fraction in the extracellular microenvironment of the rat cerebellum. J Physiol 1981;321:225–257.
109. Nicholson C. Diffusion of ions and macromolecules in the brain. In: Le Bihan D, editor. Diffusion and perfusion magnetic resonance imaging: applications to functional MRI. New York: Raven Press; 1995. p 127–131.
110. Nicholson C, Sykova E. Extracellular space structure revealed by diffusion analysis. TINS 1998;21:207–215.
111. Beaulieu C, Allen PS. Water diffusion in the giant axon of the squid: implications for diffusion-weighted MRI of the nervous system. Magn Reson Med 1994;32:579–583.
112. Cruz A, Green BG. Thermal stimulation of taste. Nature 2000; 403:889–892.
113. Meyer JW, Makris N, Bates JF, Caviness VS, Kennedy DN. MRI-based topographic parcellation of human cerebral white matter I. Technical foundations. Neuroimage 1999;9:1–17.
114. Wiegell MR, Larsson HBW, Wedeen VJ. Diffusion tensor MRI of fiber crossing in the human brain. Radiology 2000 (in press).
115. Karger J, Pfeifer H. PFG NMR self-diffusion measurements in microporous adsorbents. Magn Reson Imaging 1994;12:235–239.
116. Callaghan PT, Soderman O. Examination of the lamellar phase of aerosol OT: water using pulsed field gradient nuclear magnetic resonance. J Chem Phys 1983;87:1737.
117. Mori S, Crain BJ, Chacko VP, Van Zijl PCM. Three-dimensional tracking of axonal projections in the brain by magnetic resonance imaging. Ann Neurol 1999;45:265–269.
118. Poupon C, Mangin JF, Frouin V, et al. Regularization of MR diffusion tensor maps for tracking brain white matter bundles. New York: Springer-Verlag; 1998. p 489–498.
119. Jones DK, Simmons A, Williams SC, Horsfield MA. Non-invasive assessment of axonal fiber connectivity in the human brain via diffusion tensor MRI. Magn Reson Med 2000;42:37–41.
120. Conturo TE, Lori NF, Cull TS, et al. Tracking neuronal fiber pathways in the living human brain. Proc Natl Acad Sci USA 1999;96: 10422–10427.
121. Mori S, Kaufman WE, Pearlson GD, et al. In vivo visualization of human neural pathways by magnetic resonance imaging. Ann Neurol 2000;47:412–414.
122. Poupon C, Mangin JF, Clark CA, et al. Towards inference of human brain connectivity. Neuroimage 2000;12:184–195.
123. Stanisz GJ, Szafer A, Wright GA, Henkelman RM. An analytical model of restricted diffusion in bovine optic nerve. Magn Reson Med 1997;37:103–111.
124. Morvan D. In vivo measurement of diffusion and pseudo-diffusion in skeletal muscle at rest and after exercise. Magn Reson Imaging 1995;13:193–199.
125. Baur A, Stabler A, Bruning R, et al. Diffusion-weighted MR imaging of bone marrow: differentiation of benign versus pathologic compression fractures. Radiology 1998;207:349–356.
126. Akansel G, Haughton VM, Papke RA, Censky S. Diffusion into human intervertebral disks studied with MR and gadoteridol. AJNR 1997;18:443–445.
127. Englander SA, Ulug AM, Brem R, Glickson JD, Van Zijl PCM. Diffusion imaging of human breast. NMR Biomed 1997;10:348–352.
128. Maier CF, Paran Y, Bendel P, Rutt BK, Degani H. Quantitative diffusion imaging in implanted human breast tumors. Magn Reson Med 1997;37:576–581.
129. Maier CF, Nikolov HN, Chu KC, Chronik BA, Rutt BK. Practical design of a high-strength breast gradient coil. Magn Reson Med 1998;39:392–401.
130. Namimoto T, Yamashita Y, Sumi S, Tang Y, Takahashi M. Focal liver masses: characterization with diffusion-weighted echo-planar MR imaging. Radiology 1997;204:739–744.
131. Ichikawa T, Haradome H, Hachiya J, Nitatori T, Araki T. Diffusion-weighted MR imaging with a single-shot echoplanar sequence: detection and characterization of focal hepatic lesions. AJR 1998;170:397–402.
132. Yamashita Y, Tang Y, Takahashi M. Ultrafast MR imaging of the abdomen: echo planar imaging and diffusion-weighted imaging. J Mag Reson Imaging 1998;8:367–374.
133. Yamada I, Aung W, Himeno Y, Nakagawa T, Shibuya H. Diffusion coefficients in abdominal organs and hepatic lesions: evaluation with intravoxel incoherent motion echo-planar MR imaging. Radiology 1999;210:617–623.
134. Gilbert RJ, Reese TG, Daftary SJ, et al. Determination of lingual myoarchitecture in whole tissue by NMR imaging of anisotropic water diffusion. Am J Physiol 1998;275:G363–369.
135. Scollan DF, Holmes A, Winslow R, Forder J. Histological validation of myocardial microstructure obtained from diffusion tensor magnetic resonance imaging. Am J Physiol Heart Circ Phys 1998; 44:H2308–H2318.